ORCA – Online Research @ Cardiff

Measuring Linearity of Curves in $2D$ and $3D$

Paul L. Rosin[*]   Jovanka Pantović[†]   Joviša Žunić [‡]

Abstract

In this paper we define a new linearity measure for open curve segments in $2D$ and $3D$. The measure considers the distance of the curve end points to the curve centroid. It is simple to compute and has the basic properties that should be satisfied by any linearity measure. The new measure ranges over the interval $(0, 1]$, and produces the value 1 if and only if the measured curve is a perfect straight line segment. Also, the new linearity measure is invariant with respect to translations, rotations and scaling transformations. The new measure is theoretically well founded and, because of this, its behaviour can be well understood and predicted to some extent. This is always beneficial because it indicates the suitability of the new measure to the desired application.

Several experiments are provided to illustrate the behaviour and to demonstrate the efficiency and applicability of the new linearity measure.

Key words: Shape, curves, linearity measure, image processing.

[*]P.L. Rosin is with Cardiff University, School of Computer Science, Cardiff CF24 3AA, Wales, U.K. e-mail: Paul.Rosin@cs.cf.ac.uk;

[†]J. Pantović is with the University of Novi Sad, Faculty of Technical Sciences, 21000 Novi Sad, Serbia e-mail: pantovic@uns.ac.rs

[‡]J. Žunić is with the University of Exeter, Computer Science, Exeter EX4 4QF, U.K. e-mail: J.Zunic@ex.ac.uk

1 Introduction

Shape descriptors have been employed in many computer vision and image processing tasks (e.g. image retrieval, object classification, object recognition, object identification, etc). Different mathematical tools have been used to define the shape descriptors: algebraic invariants [14], Fourier analysis [6], morphological operations [26], integral transformations [23], statistical methods [17], fractal techniques [15], logic [27], combinatorial methods [1], multiscale approaches [9], integral invariants [16], multi-scale integral geometry [3, 4, 18], etc. Generally speaking, shape descriptors can be classified into two groups: area based descriptors and boundary based ones. Area based descriptors are more robust (i.e. less sensitive to noise or shape deformations) while boundary based descriptors are more sensitive. A preference for either type of descriptor depends on the application performed and the data available. For example low quality data would require robust descriptors (i.e. area based ones) while high precision tasks would require more sensitive descriptors (i.e. boundary based ones). In the literature so far, more attention has been paid to the area based descriptors, not only because of their robustness but also because they are easier to be efficiently estimated when working with discrete data. Due to the recent proliferation of image verification, identification and recognition systems there is a strong demand for shape properties that can be derived from their boundaries [16, 19, 30]. It is worth mentioning that some objects, like human signatures for example, are open curves by their nature and area based descriptors cannot be used for their analysis.

In this paper we deal with linearity measures that should indicate the degree to which an open curve segment differs from a perfect straight line segment. Several linearity measures for curve segments are already considered in the literature [12, 13, 29, 32, 36]. All of these measures have their strengths and their weakness. One measure performing well in one application, might have a poor performance in another. This is why multiple measures, for certain shape properties, are needed.

Perhaps the simplest way to define the linearity measure of an open curve segment is to consider the ratio between the length of the curve considered and the distance between its end points. This is a natural and simple definition which is also called the *straightness index* (or simply *straightness*) [5].

In this paper we introduce a new linearity measure for open curve segments. The new linearity measure is computed as the sum of distances of the curve end points to the curve centroid.

Both measures satisfy the following basic requirements for a linearity measure of open curve segments.

- They vary through the interval $(0, 1]$;

- They equal 1 only for straight line segments;

- They are invariant with respect to translation, rotation and scaling transformation on a curve considered.

The straightness index is simple to compute and its behaviour can be clearly predicted, i.e. we can see easily which curves have the same linearities, measured by the straightness

2

index. It is obvious that those curves whose end points and the length coincide, have the same straightness index. But the diversity of such curves is huge and the straightness index cannot distinguish among them, which could be a big drawback in certain applications (of course, in some applications it could be a desirable property). Some illustrations using simple polygonal curves are shown in Figure 1.

Figure 1: Five displayed curves (solid lines) have different linearities measured by the new measure $\mathcal{L}(\mathcal{C})$. The straightness index has the same value, equal to 1/2 for all five curves.

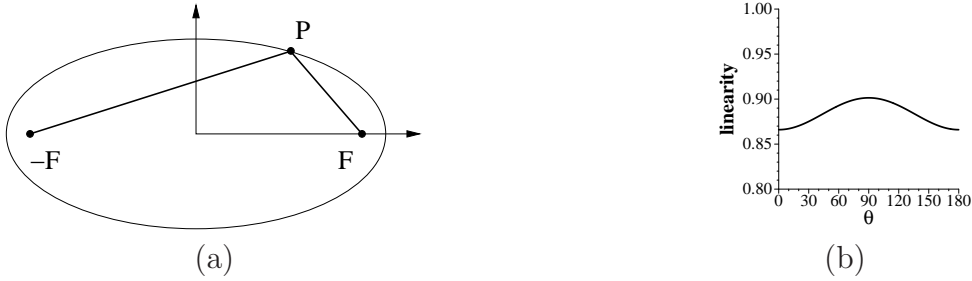Figure 2: The family of polylines $-\mathbf{FPF}$, in (a), all produce a constant straightness index, while $\mathbf{P}$ varies through the ellipse displayed. The graph in (b) plots $\mathcal{L}(\mathcal{C})$, where $\mathcal{C} = -\mathbf{FPF}$ is the same polyline as in (a), and $\theta = \angle\mathbf{FOP}$ ($\mathbf{O} = (0,0)$ is the origin).

Another example is given in figure 2 which shows two line segments constructed from the foci of an ellipse $\pm\mathbf{F}$ and a point on the ellipse $\mathbf{P}$. Since the ellipse has the property that $\overline{-\mathbf{FP}} + \overline{\mathbf{PF}}$ remains constant (while $\mathbf{P}$ varies through the ellipse), the straightness index of the polyline $-\mathbf{FPF}$ has constant value (because the polyline has constant perimeter and fixed endpoints). The proposed linearity $\mathcal{L}(\mathcal{C})$ (see Definition 2, in Section 3, for a precise definition) varies as shown in the graph computed in figure 2b (the angle θ is determined by the points $\mathbf{F}$, $\mathbf{O} = (0,0)$, and $\mathbf{P}$). This construction is used to generate a further example in figure 3 in which the spikes of the shape are modified such that all the shapes have constant straightness values but varying linearities are measured by the new measure $\mathcal{L}(\mathcal{C})$.

Of course, for any shape measure (including the linearity measure proposed in this paper) which maps the set of all planar curves onto the interval $(0,1]$, there must be infinitely many curves $\mathcal{C}$ satisfying $\mathcal{L}(\mathcal{C}) = l_0$, for some constant $l_0 \in (0,1)$. For example: the new linearity measure assigns the same value to all curves whose sum of the distances of the end points to the curve centroid is the same, the measure from [36] assigns the same value for all the curves having the same value of the boundary-based first Hu moment invariant analogue, etc. This cannot be avoided. Some examples are given in figure 4, for which not only the proposed linearity measure, but also the straightness index produces the same value.
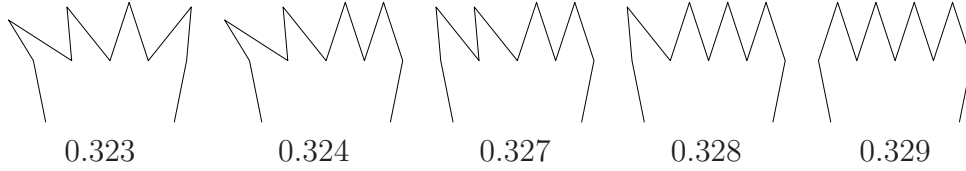
3

0.323   0.324   0.327   0.328   0.329

Figure 3: The five displayed curves have different linearities measured by the new measure $\mathcal{L}(\mathcal{C})$. The straightness index has the same value, equal to 0.209 for all five curves.

While there will exist examples of sets of shapes that have a constant linearity measure but differing straightness index values, these are not easy to synthesise since this would require constructing two or more shapes with the same perimeter length, the same distance between centroid and endpoints, but different distances between endpoints.
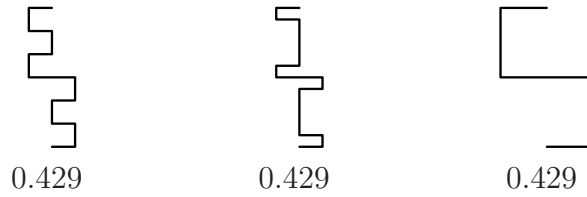

0.429   0.429   0.429

Figure 4: The linearities measured by the new measure $\mathcal{L}(\mathcal{C})$ and the straightness index all produce identical values for the three displayed curves.

Another example comparing straightness and $\mathcal{L}(\mathcal{C})$ is given in figure 5. Four examples of hands have each been modified by cropping increasing amounts off one end of the curve. As can be seen, the straightness measure could be understood as more sensitive than $\mathcal{L}(\mathcal{C})$ to the position of the curves' endpoints. The ranking by $\mathcal{L}(\mathcal{C})$ groups all the different versions of each of the four models, except for the middle two shapes in figure 5. By contrast, the ranking by the straightness index/measure is such that no grouping of three instances of any of the four hand shapes is formed, and only one grouping of two instances occurs.

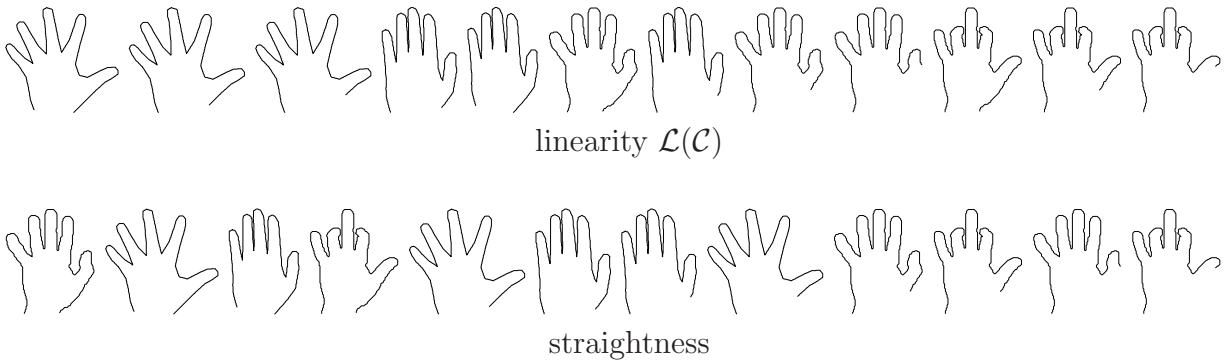linearity $\mathcal{L}(\mathcal{C})$

straightness

Figure 5: Hand outlines (with varying amounts of cropping at one end) ranked according to linearity or straightness.

In this paper we define a new linearity measure $\mathcal{L}(\mathcal{C})$ for open curve segments. The new measure satisfies the basic requirements (listed above) which are expected to be satisfied

4

for any curve linearity measure. Since $\mathcal{L}(\mathcal{C})$ considers the distance of the end points of the curve to the centroid of the curve, the new measure is also easy to compute. The fact that it uses the curve centroids implies that it takes into account a relative distribution of the curve points. The method also has a straightforward extension to $3D$.

The paper is organized as follows. Section 2 gives basic definitions and denotations. The new linearity measure for planar open curve segments is introduced in Section 3. An extension to $3D$ curves is content of Section 4. Several experiments which illustrate the behaviour and the classification power of the new linearity measure are provided in Section 5. Concluding remarks are in Section 6.

2 Definitions and Denotations

In this paper we deal with both $2D$ and $3D$ curve segments.

Without loss of generality, throughout the paper, it will be assumed (even if not mentioned) that every curve $\mathcal{C}$ has length equal to 1 and is given in an arc-length parametrization. I.e., planar curve segment $\mathcal{C}$ is represented as:

$$x = x(s), \qquad y = y(s), \quad \text{where} \quad s \in [0, 1].$$

The parameter s measures the distance of the point $(x(s), y(s))$ from the curve start point $(x(0), y(0))$, along the curve $\mathcal{C}$.

A $3D$ curve segment $\mathcal{C}$ is represented as:

$$x = x(s), \qquad y = y(s), \qquad z = z(s), \quad \text{where} \quad s \in [0, 1].$$

Analogously as in the planar case above, s measures the distance of the point $(x(s), y(s), z(s))$ from the curve start point $(x(0), y(0), z(0))$, along the curve $\mathcal{C}$.

The centroid of a given planar curve $\mathcal{C}$ will be denoted by $(x_{\mathcal{C}}, y_{\mathcal{C}})$ and computed as

$$(x_{\mathcal{C}}, y_{\mathcal{C}}) \;=\; \left(\int_{\mathcal{C}} x(s) \; ds, \; \int_{\mathcal{C}} y(s) \; ds \right). \tag{1}$$

The centroid of a given $3D$ curve $\mathcal{C}$ will be denoted by $(x_{\mathcal{C}}, y_{\mathcal{C}}, z_{\mathcal{C}})$ and computed as

$$(x_{\mathcal{C}}, y_{\mathcal{C}}, z_{\mathcal{C}}) \;=\; \left(\int_{\mathcal{C}} x(s) \; ds, \; \int_{\mathcal{C}} y(s) \; ds, \; \int_{\mathcal{C}} y(s) \; ds \right). \tag{2}$$

Taking into account that the length of $\mathcal{C}$ is assumed to be equal to 1, we can see that the coordinates of curve centroid, as defined in both (1) and (2), are the average values of the coordinates of all the curve points.

As usual, $\mathbf{d}_2(A, B)$ will denote the Euclidean distance between the points A and B.

As mentioned, we introduce a new linearity measure $\mathcal{L}(\mathcal{C})$ which assigns to each curve $\mathcal{C}$ a number from the interval $(0, 1]$. The curve $\mathcal{C}$ is assumed to have the length 1. More precisely, any appearing curve will be scaled by the factor which equals the length of it before the processing. So, an arbitrary curve $\mathcal{C}_a$ would be replaced with the curve $\mathcal{C}$ defined by

$$\mathcal{C} \;=\; \frac{1}{\int_{\mathcal{C}_a} ds} \cdot \mathcal{C}_a \;=\; \left\{ \left(\frac{x}{\int_{\mathcal{C}_a} ds}, \; \frac{y}{\int_{\mathcal{C}_a} ds} \right) \mid (x, y) \in \mathcal{C}_a \right\}$$

i.e. in 3D with

$$\mathcal{C} \;=\; \frac{1}{\int_{\mathcal{C}_a} ds} \cdot \mathcal{C}_a \;=\; \left\{ \left(\frac{x}{\int_{\mathcal{C}_a} ds}, \; \frac{y}{\int_{\mathcal{C}_a} ds}, \; \frac{z}{\int_{\mathcal{C}_a} ds} \right) \mid (x, y, z) \in \mathcal{C}_a \right\}.$$

Shape descriptors/measures are very useful for discrimination among the objects – in this case open curve segments. A particular attention can be given to the shape descriptors having a clear geometric meaning, because shape measures assigned to such descriptors have a predictable behaviour. This is an advantage because the suitability of a certain measure to a particular shape-based task (object matching, object classification, etc) can be predicted to some extent. On the other hand, a shape measure assigns to each object (here curve segment) just a single number. In order to increase the performance of computational tasks based on the shape characteristics comparison, a common approach is to assign a graph (instead of a number) to each object. E.g. such approaches define *shape signature* descriptors, which are also 'graph' representations of planar shapes, often used in shape analysis tasks [10, 37].

We will apply a similar idea here as well. To compare objects considered we use *linearity plots* (the approach is taken from [36] and more details can be found therein) to provide more information than a single linearity measurement. The idea is to compute linearity incrementally, i.e. to compute linearity of sub-segments of $\mathcal{C}$ determined by the start point of $\mathcal{C}$ and another point which moves along the curve $\mathcal{C}$ from the beginning of $\mathcal{C}$ to the end of $\mathcal{C}$. The linearity plot $\mathrm{P}(\mathcal{C})$, associated with the given curve $\mathcal{C}$ is formally defined as follows.

Definition 1 *Let $\mathcal{C}$ be a curve given in an arc-length parametrization: $x = x(s)$, $y = y(s)$, (i.e. $x = x(s)$, $y = y(s)$, $z = z(s)$ in 3D) and $s \in [0,1]$. Let $\mathbf{A}(s)$ be the part of the curve $\mathcal{C}$ bounded by the starting point $(x(0), y(0))$ (i.e. $(x(0), y(0), z(0))$) and by the point $(x(s), y(s)) \in \mathcal{C}$ (i.e. $(x(s), y(s), z(s)) \in \mathcal{C}$). Then, for a linearity measure $\mathcal{L}$, the linearity plot $\mathrm{P}(\mathcal{C})$ is defined by:*

$$\mathrm{P}(\mathcal{C}) = \{(s, \mathcal{L}(\mathbf{A}(s)) \mid s \in [0,1]\}. \tag{3}$$

We also will use the *reverse linearity plot* $\mathrm{P}_{rev}(\mathcal{C})$ defined as:

$$\mathrm{P}_{rev}(\mathcal{C}) = \{(s, \mathcal{L}(\mathbf{A}_{rev}(1-s)) \mid s \in [0,1]\}, \tag{4}$$

where $\mathbf{A}_{rev}(1-s)$ is the segment of the curve $\mathcal{C}$ determined by the end point $(x(1), y(1))$ (i.e. $(x(1), y(1), z(1))$ in 3D) of $\mathcal{C}$ and the point which moves from the end point of $\mathcal{C}$, to the start point of $\mathcal{C}$, along the curve $\mathcal{C}$. In other words, $\mathrm{P}_{rev}(\mathcal{C})$ is the linearity plot of the curve $\mathcal{C}'$ which coincides with the curve $\mathcal{C}$ but the start (end) point of $\mathcal{C}$ is the end (start) point of $\mathcal{C}'$. A parametrization of $\mathcal{C}'$ can be obtained by replacing the parameter s, in the parametrization of $\mathcal{C}$, by a new parameter s' such that $s' = 1 - s$. Obviously such a defined s' measures the distance of the point $(x(s'), y(s'))$ (i.e. $(x(s'), y(s'), z(s'))$) from the starting point $(x(s' = 0), y(s' = 0))$ (i.e. $(x(s' = 0), y(s' = 0), z(s' = 0))$) of $\mathcal{C}'$ along the curve $\mathcal{C}'$, as s' varies through the interval $[0, 1]$.

For the sake of simplicity, in the experimental section (Section 5), the function which corresponds to the linearity plot $\mathrm{P}(\mathcal{C})$ will be denoted by $\mathrm{P}(\mathcal{C})(s)$, with $s \in [0, 1]$. Similarly, the function which corresponds to the reverse linearity plot $\mathrm{P}_{rev}(\mathcal{C})(s)$ will be denoted by $\mathrm{P}_{rev}(\mathcal{C})(s)$.

3 New Linearity Measure for Open Curve Segments

In this section we introduce a new linearity measure for open planar curve segments. In the next section we extend the results to the $3D$ case.

We start with the following theorem which says that amongst all curves having the same length, straight line segments have the largest sum of distances between the curve end points to the curve centroid. This result will be exploited to define the new linearity measure for open curve segments.

Theorem 1 *Let $\mathcal{C}$ be an open curve segment given in an arc-length parametrization $x = x(s)$, $y = y(s)$, and $s \in [0,1]$. The following statements hold:*

(a) *The sum of distances of the end points $(x(0), y(0))$ and $(x(1), y(1))$ from the centroid $(x_{\mathcal{C}}, y_{\mathcal{C}})$ of the curve $\mathcal{C}$ is bounded from above by 1, i.e.:*

$$\mathbf{d}_2((x(0), y(0)), (x_{\mathcal{C}}, y_{\mathcal{C}})) \ + \ \mathbf{d}_2((x(1), y(1)), (x_{\mathcal{C}}, y_{\mathcal{C}})) \ \leq \ 1. \qquad (5)$$

(b) *The upper bound established by the previous item is reached by the straight line segment and, consequently, cannot be improved.*

Proof. Let $\mathcal{C}$ be a curve given in an arc-length parametrization: $x = x(s)$ and $y = y(s)$, with $s \in [0,1]$, and let $S = (x(0), y(0))$ and $E = (x(1), y(1))$ be the end points of $\mathcal{C}$. We can assume, without loss of generality, that the curve segment $\mathcal{C}$ is positioned such that

- the end points S and E belong to the x-axis (i.e. $y(0) = y(1) = 0$), and

- S and E are symmetric with respect to the origin (i.e. $-x(0) = x(1)$),

as illustrated in Fig. 6. Furthermore, let $\mathcal{E} = \{X = (x, y) \mid \mathbf{d}_2(X, S) + \mathbf{d}_2(X, E) \ = \ 1\}$ be
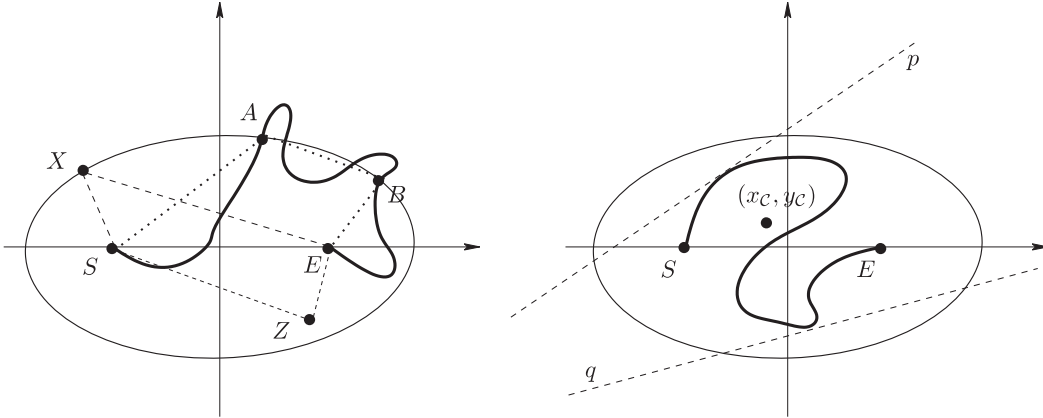

Figure 6: Denotations in the proof of Theorem 1 are illustrated above.

an ellipse which consists of points whose sum of distances to the points S and E is equal to 1. Now, we prove (a) in two steps.

(i) First, we prove that the curve $\mathcal{C}$ and the ellipse $\mathcal{E}$ do not have more than one intersection point (i.e. $\mathcal{C}$ belongs to the closed region bounded by $\mathcal{E}$).

This will be proven by a contradiction. So, let us assume the contrary, that $\mathcal{C}$ intersects $\mathcal{E}$ at k ($k \geq 2$) points: $(x(s_1), y(s_1))$, $(x(s_2), y(s_2))$, ..., $(x(s_k), y(s_k))$, where $0 < s_1 < s_2 < \ldots < s_k < 1$. Let $A = (x(s_1), y(s_1))$ and $B = (x(s_k), y(s_k))$.

Now, by using the triangle equality and the fact that the length of any path between two points is bounded below by the Euclidean distance between these two points, we derive the contradiction $1 < 1$, as follows:

$$
\begin{aligned}
1 &= \mathbf{d}_2(S, A) + \mathbf{d}_2(A, E) < \mathbf{d}_2(S, A) + \mathbf{d}_2(A, B) + \mathbf{d}_2(B, E) \\
&\leq \int_{\widehat{SA}} ds + \int_{\widehat{AB}} ds + \int_{\widehat{BE}} ds = \int_{\mathcal{C}} ds = 1.
\end{aligned}
\tag{6}
$$

So, $\mathcal{C}$ and $\mathcal{E}$ do not have more than one intersection point, implying that $\mathcal{C}$ lies in the closed region bounded by $\mathcal{E}$.

(ii) Second, we prove that the centroid of $\mathcal{C}$ does not lie outside of $\mathcal{E}$. The proof follows easily, from the following two remarks:

 - The convex hull $CH(\mathcal{C})$ of $\mathcal{C}$ is the smallest convex set which includes $\mathcal{C}$ and, consequently, is a subset of the region bounded by $\mathcal{E}$.

 - The centroid of $\mathcal{C}$ lies in the convex hull $CH(\mathcal{C})$ of $\mathcal{C}$ because it belongs to every half plane which includes $\mathcal{C}$ (the intersection of such half planes is actually the convex hull of $\mathcal{C}$ (see [31]));

Finally, since $(x_\mathcal{C}, y_\mathcal{C}) \in CH(\mathcal{C}) \subset region\_bounded\_by\_\mathcal{E}$ is proven, we deduce

$$\mathbf{d}_2((x(0), y(0)), (x_\mathcal{C}, y_\mathcal{C})) + \mathbf{d}_2((x(1), y(1)), (x_\mathcal{C}, y_\mathcal{C})) \leq 1.$$

This establishes **(a)**.

To prove **(b)** it is enough to notice that if $\mathcal{C}$ is a straight line segment of length 1, then the sum of its end points to the centroid of $\mathcal{C}$ is 1. $\qquad\square$

Now, motivated by the results of Theorem 1, we give the following definition for a new linearity measure $\mathcal{L}(\mathcal{C})$ for open curve segments.

Definition 2 *Let $\mathcal{C}$ be an open curve segment. Then, the linearity measure $\mathcal{L}(\mathcal{C})$ of $\mathcal{C}$ is defined as the sum of distances between the centroid $(x_\mathcal{C}, y_\mathcal{C})$ of $\mathcal{C}$ and the end points of $\mathcal{C}$. I.e.:*

$$\mathcal{L}(\mathcal{C}) = \mathbf{d}_2((x(0), y(0)), (x_\mathcal{C}, y_\mathcal{C})) + \mathbf{d}_2((x(1), y(1)), (x_\mathcal{C}, y_\mathcal{C})) \tag{7}$$

where $x = x(s)$, $y = y(s)$, $s \in [0, 1]$ is an arc-length representation of $\mathcal{C}$.

The following theorem summarizes desirable properties of $\mathcal{L}(\mathcal{C})$.

Theorem 2 *The linearity measure $\mathcal{L}(\mathcal{C})$ has the following properties:*

(i) $\mathcal{L}(\mathcal{C}) \in (0,1],\quad$ *for all open curve segments $\mathcal{C}$;*

(ii) $\mathcal{L}(\mathcal{C}) = 1 \quad\Leftrightarrow\quad \mathcal{C}$ *is a straight line segment;*

(iii) $\mathcal{L}(\mathcal{C})$ *is invariant with respect to the similarity transformations.*

Proof. Item **(i)** is a direct consequence of Theorem 1.

To prove **(ii)** we will use the same notations as in the proof of Theorem 1 and give a proof by contradiction. So, let assume the following:
– the curve $\mathcal{C}$ differs from a straight line segment, i.e., $\mathbf{d}_2(S, E) < 1$, and
– the sum of distances between the end points, and the centroid of $\mathcal{C}$ is 1, i.e., $(x_{\mathcal{C}}, y_{\mathcal{C}})$ lies on the ellipse $\mathcal{E} = \{X = (x, y) \mid \mathbf{d}_2(X, S) + \mathbf{d}_2(X, E) = 1\}$.

Further, it would mean that there are points of the curve $\mathcal{C}$ belonging to both half-planes determined by the tangent on the ellipse $\mathcal{E}$ passing through the centroid of $\mathcal{C}$. This would contradict the fact that $\mathcal{C}$ and $\mathcal{E}$ do not have more than one intersection point (what was proven as a part of the proof of Theorem 1).

To prove item **(iii)** it is enough to notice that translations and rotations do not change the distance between the centroid and the end points. Since $\mathcal{C}$ is represented by using an arc-length parametrization: $x = x(s)$, $y = y(s)$, with $s \in [0, 1]$, the new linearity measure $\mathcal{L}(\mathcal{C})$ is invariant with respect to scaling transformations as well. $\qquad\square$

4 Linearity of Open Curve Segments in $3D$

In this section we extend the linearity measure $\mathcal{L}(\mathcal{C})$ of planar curve segments $\mathcal{C}$ to $3D$ curve segments. As in the second section which introduces basic definitions and denotations, we will use the same notation: $\mathcal{C}$ for the $3D$ curves and $\mathcal{L}(\mathcal{C})$ for their linearity measures, but this will not cause any confusion. Again, we will assume that all curves $\mathcal{C}$ have length 1 and are represented in an arc-length parametrization $x = x(s)$, $y = y(s)$, $z = z(s)$, $s \in [0, 1]$, where the parameter s is the distance between the curve start point $(x(0), y(0), z(0))$ and the point $(x(s), y(s), z(s)) \in \mathcal{C}$ along the curve $\mathcal{C}$. The centroid $(x_{\mathcal{C}}, y_{\mathcal{C}}, z_{\mathcal{C}})$ of $\mathcal{C}$ is defined as in (2).

The following theorem is an analogue of Theorem 1.

Theorem 3 *Let $\mathcal{C}$ be an open curve given in an arc-length parametrization $x = x(s)$, $y = y(s)$, $z = z(s)$ and $s \in [0, 1]$. Then the following statements hold:*

(a) *The sum of distances of the end points $S = (x(0), y(0), z(0))$ and $E = (x(1), y(1), z(1))$ from the centroid $\mathbf{C}_{\mathcal{C}} = (x_{\mathcal{C}}, y_{\mathcal{C}}, z_{\mathcal{C}})$ of $\mathcal{C}$ is bounded from above by 1, i.e.:*

$$\mathbf{d}_2(S, \mathbf{C}_{\mathcal{C}}) + \mathbf{d}_2(E, \mathbf{C}_{\mathcal{C}}) \leq 1. \tag{8}$$

(b) *The upper bound established by (8) is reached by the straight line segment and, consequently, cannot be improved.*

Proof. We use the same idea and denotations as in the proof of Theorem 1. So, let $S = (x(0), y(0), z(0))$ and $E = (x(1), y(1), z(1))$, and let $\mathcal{C}$ be positioned such that
– the points S and E belong to the x-axis, and
– the points S and E are symmetric with respect to the origin.

We give a short proof of **(a)** because of an analogy to the $2D$ case. The proof of **(b)** is omitted since the statement of **(b)** is easy to verify.

(a) Let $\mathcal{E} = \{X = (x, y, z) \mid \mathbf{d}_2(X, S) + \mathbf{d}_2(X, E) = 1\}$. Similarly as in $2D$ case, we can prove that the curve $\mathcal{C}$ and the ellipsoid $\mathcal{E}$ do not have more than one intersection point (again, a proof by contradiction can be given, by using an ellipsoid instead of the ellipse).

Furthermore, as in the proof in the $2D$ case, $CH(\mathcal{C})$ is a subset of the region bounded by $\mathcal{E}$. Also, $(x_\mathcal{C}, y_\mathcal{C}, z_\mathcal{C}) \in CH(\mathcal{C})$ because the centroid of $\mathcal{C}$ lies in every half space which includes $\mathcal{C}$. The intersection of such half spaces is actually the convex hull of $\mathcal{C}$.

Finally, since the centroid of $\mathcal{C}$ lies inside the region bounded by $\mathcal{E}$, the sum of its distances to the end points is not bigger than 1, which proves **(a)**. $\qquad\square$

Based on the previous theorem, we extend Definition 2 to open curve segments in $3D$.

Definition 3 *Let $\mathcal{C}$ be an open curve segment in $3D$. Then, the linearity measure $\mathcal{L}(\mathcal{C})$ of $\mathcal{C}$ is defined as the sum of distances between the centroid $(x_\mathcal{C}, y_\mathcal{C}, z_\mathcal{C})$ of $\mathcal{C}$ and the end points of $\mathcal{C}$.*

The desirable properties of $\mathcal{L}(\mathcal{C})$ listed in Theorem 2 hold also in $3D$. We give the next theorem without proof because it is identical to the proof of Theorem 2.

Theorem 4 *Let $\mathcal{C}$ be an open curve segment in $3D$. The following properties hold:*

(i) $\mathcal{L}(\mathcal{C}) \in (0, 1]$;

(ii) $\mathcal{L}(\mathcal{C}) = 1 \quad \Leftrightarrow \quad \mathcal{C}$ *is a straight line segment;*

(iii) $\mathcal{L}(\mathcal{C})$ *is invariant with respect to similarity transformations.*

5 Experiments

In this section we provide several experiments in order to illustrate the behaviour and efficiency of the linearity measure in both $2D$ and $3D$.

First experiment ($2D$): Illustration. To demonstrate how various shapes produce a range of linearity values, figure 7 shows handwritten digits (0–9) from the training set captured by Alimoğlu and Alpaydin [2] plotted in a $2D$ feature space of linearity $\mathcal{L}(\mathcal{C})$ versus rectilinearity $\mathcal{R}_1(\mathcal{C})$ [34].[1] In figure 7a the first two samples of each handwritten digit

---

[1]The rectilinearity of a shape S is calculated by Žunić and Rosin [34] as follows: $\frac{\pi}{\pi - 2\sqrt{2}} \left(\max\limits_{\alpha \in [0, 2\pi]} \frac{\mathcal{P}_1(S, \alpha)}{\sqrt{2}\mathcal{P}_2(X)} - \frac{2\sqrt{2}}{\pi} \right)$ where $\mathcal{P}_2(S)$ is the perimeter of S under the L_2 norm, and $\mathcal{P}_1(X, \alpha)$ is the L_1 perimeter obtained by first rotating S by the angle α with the origin as the centre of rotation.
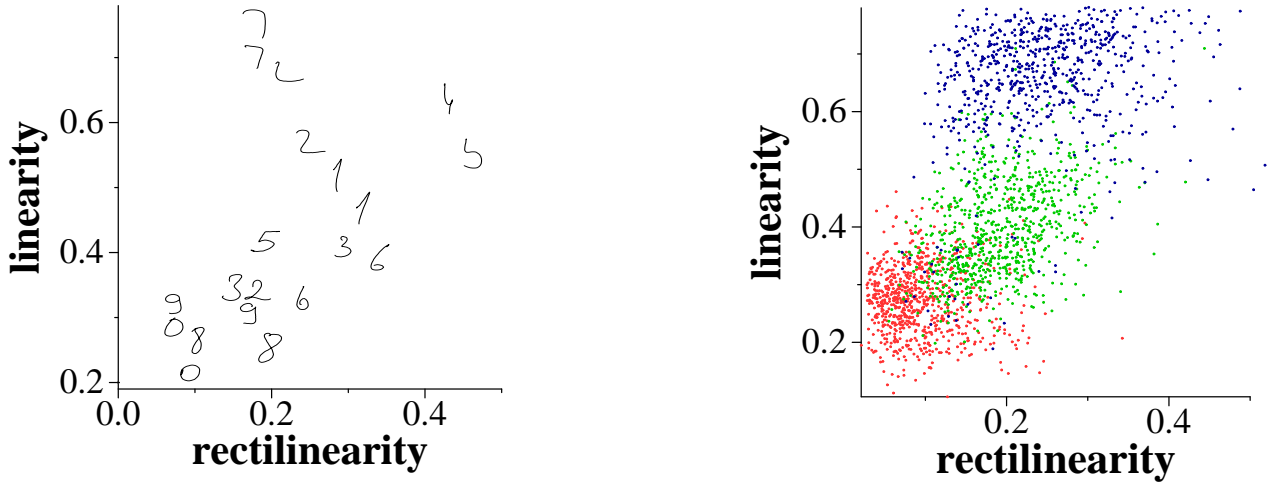
Figure 7: Handwritten digits ordered by linearity and rectilinearity. (a) Two samples of each digit; (b) All training digits 0, 2, 7 plotted as red, green, blue points.

is shown. Despite the variability of hand writing, most pairs of the same digit are reasonably clustered. The major separations occur for:

– "2" since only one instance has a loop in the middle;

– "4" since the instance next to the pair of "7"s is missing the vertical stroke and consequently looks very similar to a "7" rotated by 180°;

– "5" since the uppermost right instance is missing the horizontal stroke.

From the full training set of 7485 characters three digits are selected (2267 samples) and plotted in figure 7b in order to show more comprehensively that linearity can be used to provide a reasonable separation of classes in feature space. Of course, by augmenting the feature vector better classification can be obtained. For instance, using all 10 digits from the full training set, and a set of seven Hu moment invariants [14] and six further moment invariants [21] as features to train a nearest neighbour classifier with Mahalanobis distances, the classification accuracy on the independent test set (3493 digits) is 86.5%, which is improved by adding linearity measure $\mathcal{L}(\mathcal{C})$ as a feature to an accuracy of 90.0%. The straightness index was also evaluated, and improved classification accuracy to 91.50%. Examining the mismatches encountered in the classification step when using linearity reveals that these are mainly due to some instances of "5" and "0" having very similar linearity values, whereas their straightness values are more distinct (see figure 8). Of course, there are also examples in which the linearity values are more discriminative than the corresponding straightness values, e.g. the "6" and "1" in figure 8, but these are less frequent in this data set.

Figure 9 provides some examples of pairs of curves which produce identical (up to 6 decimal places) linearity or straightness values. From the combined set of 10978 digits, there were 114 pairs with identical linearity values, and 109 pairs had identical straightness values (i.e. about 2%). Note that these sets did not overlap; i.e. no pair of digits had both identical linearity and straightness values.
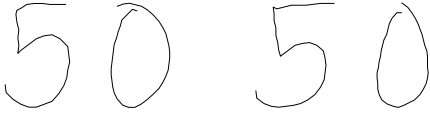
11

linearity:	0.373	0.348	0.422	0.427	0.411	0.355	0.416	0.288
straightness:	0.368	0.074	0.421	0.039	0.298	0.306	0.232	0.288

misclassified by linearity   **misclassified by straightness**

Figure 8: Misclassification of digits using moments and linearity or moments and straightness. For each pair of digits the first digit is the test shape and the second digit is the best match from the training set.
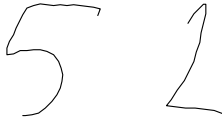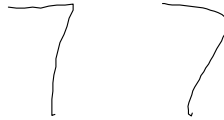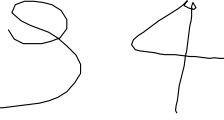

| 0.176291 | 0.176291 | 0.300917 | 0.300917 | 0.500180 | 0.500180 | 0.702861 | 0.702861 |
| 0.044741 | 0.048905 | 0.299453 | 0.297275 | 0.467512 | 0.476084 | 0.637481 | 0.633180 |

| 0.404425 | 0.260906 | 0.352286 | 0.380776 | 0.401095 | 0.407330 | 0.695872 | 0.630343 |
| 0.000000 | 0.000000 | 0.244700 | 0.244700 | 0.400808 | 0.400808 | 0.627875 | 0.627875 |

Figure 9: Examples of pairs of curves which produce identical (up to 6 decimal places) values for linearity (upper row) or straightness (lower row). Below each digit is its linearity value followed by its straightness index.

For each of the 10 classes of digits the correlation between the linearity and straightness values that were computed for all the training and test data are shown in table 1. It can be seen that linearity and straightness are highly correlated for many digits, which is to be expected since they are measuring the same shape characteristic, even thought they are capturing different aspects of it. In contrast, for those digits which are made up from closed (or in practise, almost closed) curves, and therefore have low linearity and straightness values, the two measures are essentially uncorrelated.

digit	0	1	2	3	4	5	6	7	8	9
ρ	-0.075	0.832	0.832	0.945	0.878	0.984	0.949	0.959	-0.022	0.925

Table 1: Pearson's correlation coefficient ρ between the linearity and straightness measures for 10978 handwritten digits.

Second experiment ($3D$): Illustration. Figure 10 demonstrates the measure on some simple synthetic $3D$ curves, and it can be seen how the measured linearity $\mathcal{L}(\mathcal{C})$ decreases as

the curves become more convoluted (increasing abscissa in the graph). In particular see the Hilbert curve example in which curve's complexity increases substantially as the number of levels increases. In addition, when the helix is squashed along its length then the linearity decreases as expected (dotted line versus solid line in figure 10(a).
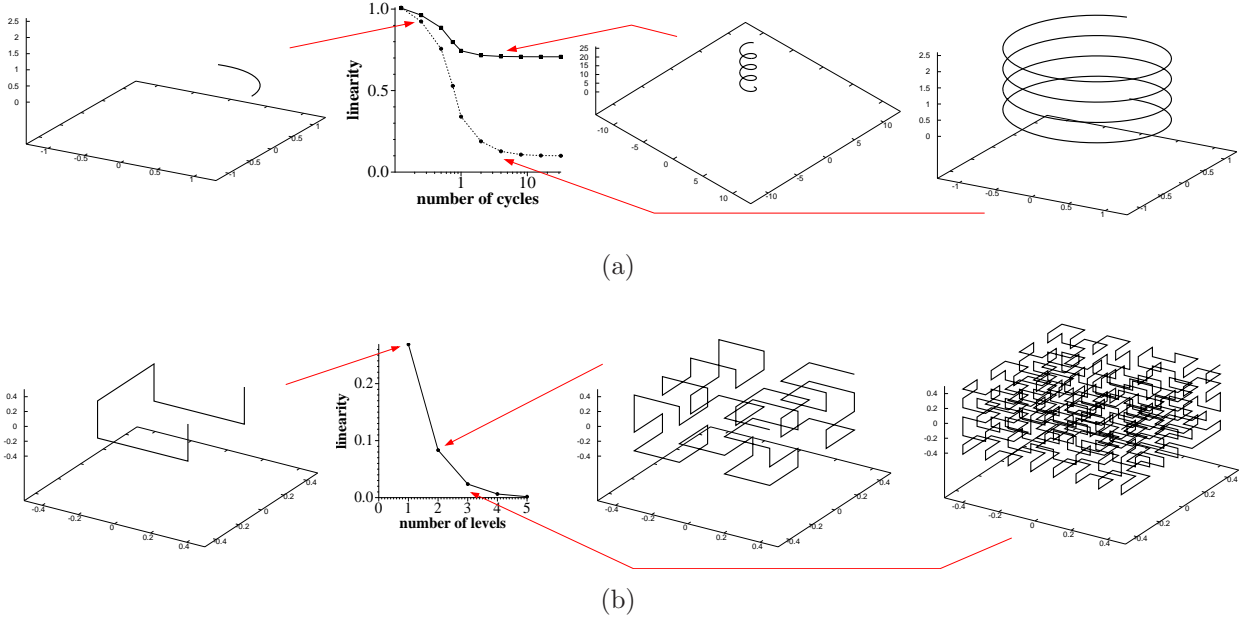

(a)

(b)

Figure 10: Linearity computed for $3D$ curves. (a) helix: $x(t) = \sin(t), y(t) = \cos(t), z = t$ (solid line) and $x(t) = \sin(t), y(t) = \cos(t), z = t/10$ (dotted line); (b) Hilbert curve.

Figure 11 compares the behaviour of the linearity and straightness values as increasing lengths of helix are traced out. It can be seen that the straightness index is sensitive to the varying position of the endpoint, producing an undesirable oscillating pattern, whereas the measured linearity $\mathcal{L}(\mathcal{C})$ decreases monotonically as the helix extends. This demonstration of the sensitivity of the straightness index reinforces the previous example given in figure 5.
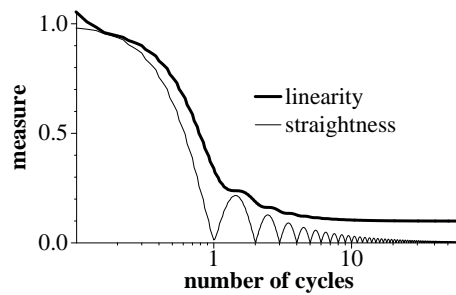
Figure 11: Linearity and straightness computed for 3D helix.

Third experiment ($2D$): Filtering edges.
Figure 12 shows the application of the linearity to filtering edges. The edges were extracted from the images using the Canny detector [7], connected into curves, and then

13
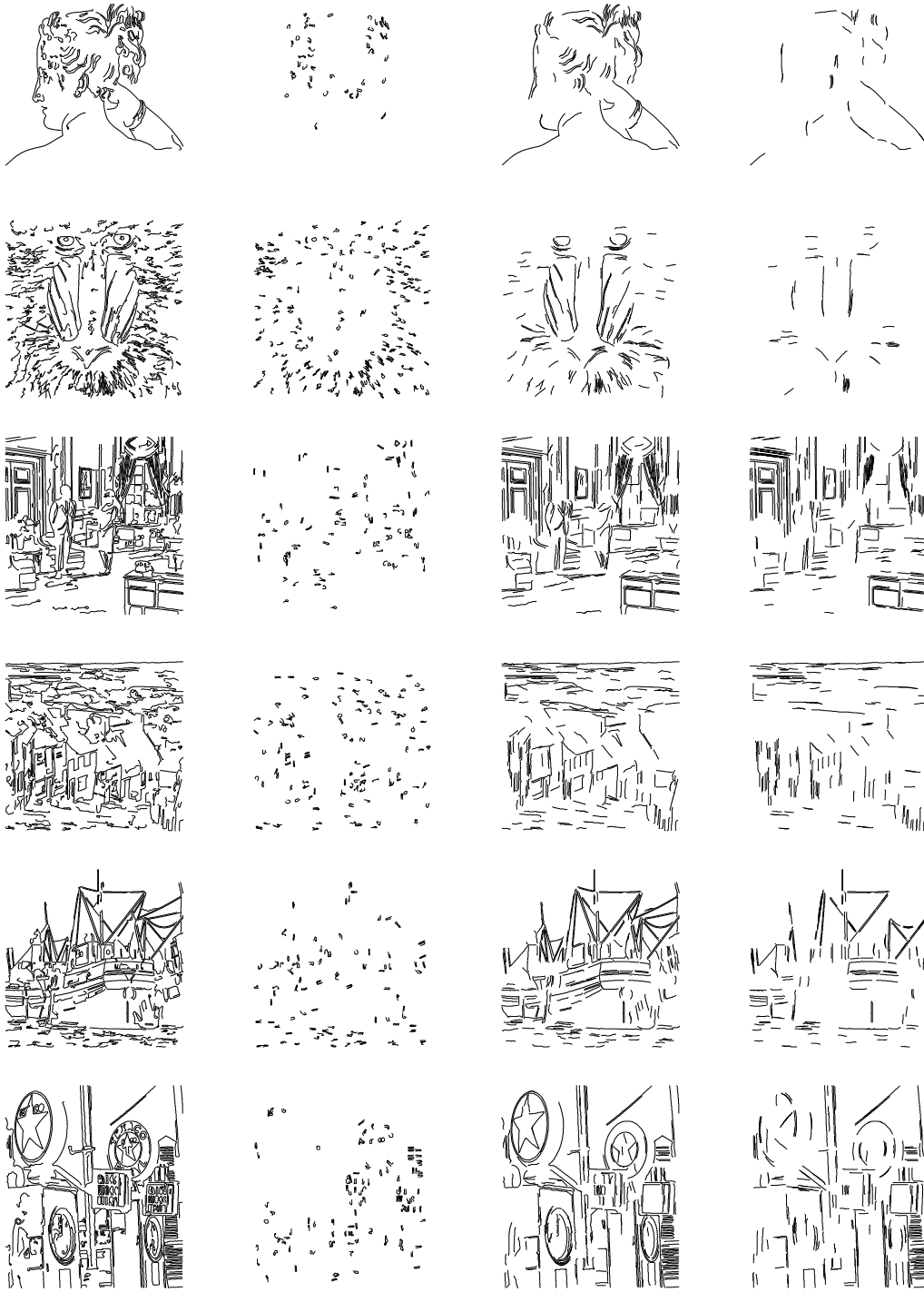
Figure 12: Filtering connected edges by linearity. Left/first column: connected edges (minimum length: 25 pixels); second column: sections of curve with $\mathcal{L}(\mathcal{C}) < 0.5$; third column: sections of curve with $\mathcal{L}(\mathcal{C}) > 0.9$; fourth column: sections of curve with $\mathcal{L}(\mathcal{C}) > 0.95$.

thresholded according to total edge magnitude and length [24]. Linearity was measured in local sections of curve of length 25, and sections above (or below) a linearity threshold were retained. It can be seen that retaining sections of curve with $\mathcal{L}(\mathcal{C}) < 0.5$ finds small noisy or corner sections. Keeping sections of curve with $\mathcal{L}(\mathcal{C}) > 0.9$ or $\mathcal{L}(\mathcal{C}) > 0.95$ identifies most of the significant structures in the image.

(a)   (b)   (c)
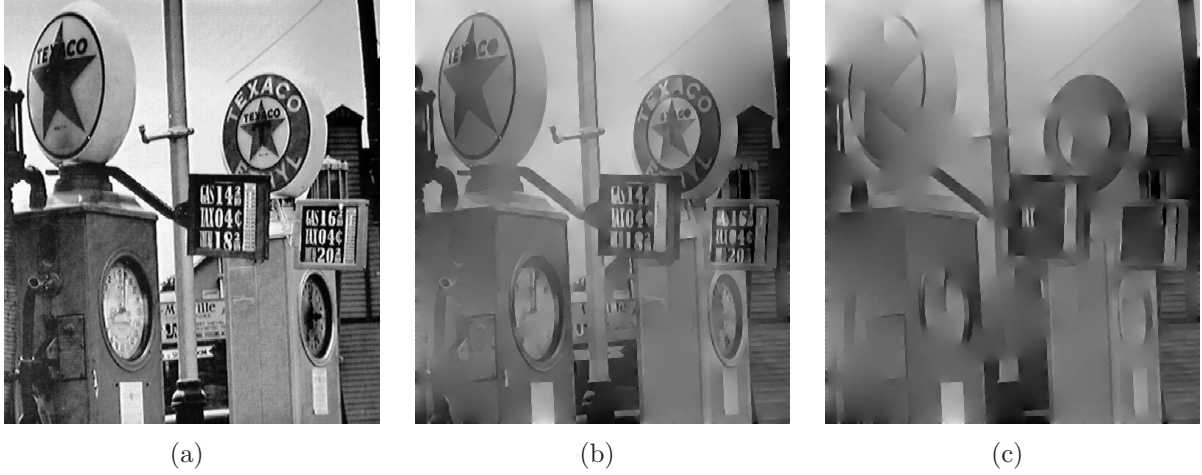
Figure 13: Reconstructing the image from its filtered edges. (a) original intensity image; (b) image reconstructed using all connected edges (minimum length: 25 pixels); (c) image reconstructed using sections of curve with $\mathcal{L}(\mathcal{C}) > 0.95$.

Experiments are also shown in which Poisson image reconstruction is performed from the image gradients [22]. In figure 13(b) all the connected edges with minimum length of 25 pixels (shown at the bottom of the first column in figure 12) have been used as a mask to eliminate all other edges before image reconstruction was performed. Some fine detail has been removed in the reconstructed image; this is to be expected since small and weak edges have been removed in the pre-processing stage. When linearity filtering is also applied to these pre-processed edges, and only edges corresponding to sections of curve with $\mathcal{L}(\mathcal{C}) > 0.95$ are used (i.e. the original edge map is masked with the edges shown at the bottom of the fourth column in figure 13), then the image reconstruction retains only regions that are locally linear structures (including sections of large circular objects).

Fourth experiment ($2D$): Signature verification. For the second application we use data from Munich and Perona [20] to perform signature verification. The data consists of pen trajectories for 2911 genuine signatures taken from 112 subjects, plus five forgers provided a total of 1061 forgeries across all the subjects. Examples of corresponding genuine and forged signatures are shown in figure 14. To compare signatures we use the linearity plots defined by (3) and (4) to provide more information than a single linearity measurement. Linearity plot examples are in figure 15 (additional examples for linearity plots based on the $3D$ linearity measure are in figure 17 given below).
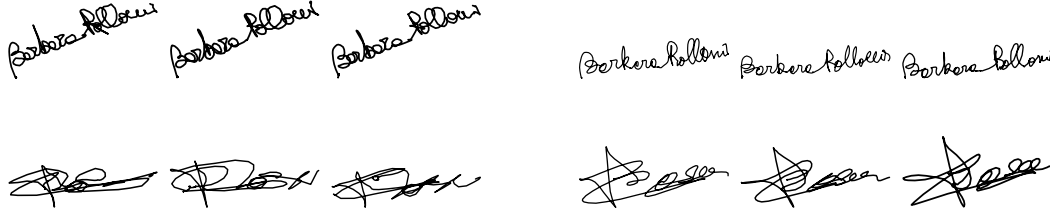
Figure 14: Examples of genuine (leftmost three) and forged (rightmost three) signatures.
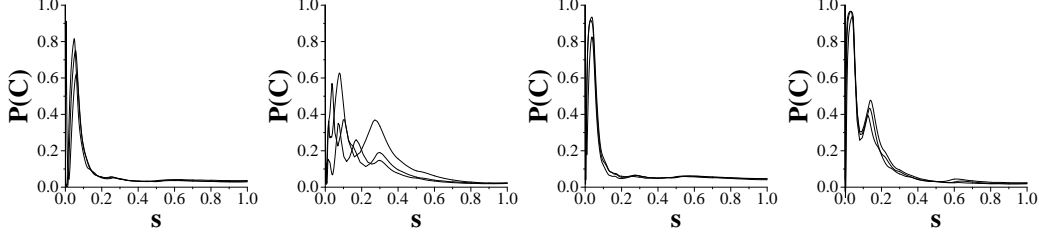

Figure 15: Examples of linearity plots for the genuine signatures (leftmost two columns) and the forged signatures (rightmost two columns) in figure 14. Linearity plots are provided for $2D$ versions of the signatures.

A straightforward idea is that the quality of match between signatures $\mathcal{C}_1$ and $\mathcal{C}_2$ is measured by the difference/distance between the linearity plots $P(\mathcal{C}_1)$ and $P(\mathcal{C}_2)$ (i.e. functions $P(\mathcal{C}_1)(s)$ and $P(\mathcal{C}_2)(s)$, with $s \in [0,1]$). This difference can be measured by the area bounded by the linearity plots $P(\mathcal{C}_1)$ and $P(\mathcal{C}_2)$ and by the vertical lines $s = 0$ and $s = 1$. In other words, the difference between signatures $\mathcal{C}_1$ and $\mathcal{C}_2$ can be measured by the quantity[2]

$$\int_{s=0}^{1} |P(\mathcal{C}_1)(s) - P(\mathcal{C}_2)(s)| \ ds. \tag{9}$$

But such a measure, for the difference between signatures $\mathcal{C}_1$ and $\mathcal{C}_2$, is not most appropriate in the situation considered here. Note that the linearity plots tend to level off by about $s = 0.5$. This is a consequence of it becoming progressively less likely that a shape remains straight along its complete length.[3] Since this means that the latter part of the linearity plots consequently contain limited discriminatory power we also consider traversing the curve in reverse direction, i.e. by considering the reverse linearity plots $P_{rev}(\mathcal{C}_1)$ and $P_{rev}(\mathcal{C}_2)$. The difference/distance of two signatures $\mathcal{C}_1$ and $\mathcal{C}_2$ is now determined as a combination of the two matches (see (9)):

$$\text{area}\left(P(\mathcal{C}_1), P(\mathcal{C}_2)\right) + \text{area}\left(P_{rev}(\mathcal{C}_1), P_{rev}(\mathcal{C}_2)\right) \ =$$

---

[2]Rather than measure the difference between points in the linearity plots at directly corresponding arc lengths, we also considered performing dynamic time warping on pairs of linearity plots to align them more closely to each other. However, we found this to degrade the results rather than improve them. In addition, the computation time substantially increased.

[3]Not all shapes will have linearity plots that level off like the examples in figure 15. Consider for instance a curve that starts at one end as a spiral, and then continues into a long straight line. Traversing from the spiral end, the linearity plot will initially sharply decrease, and then (once the straight section is encountered) monotonically increase.

$$\int_0^1 |\mathrm{P}(\mathcal{C}_1)(s) - \mathrm{P}(\mathcal{C}_2)(s)| \; ds \;\; + \;\; \int_0^1 |\mathrm{P}_{rev}(\mathcal{C}_1)(s) - \mathrm{P}_{rev}(\mathcal{C}_2)(s)| \; ds \qquad (10)$$

and we achieve better results by combining the two linearity plot differences.

Nearest neighbour matching is then performed on all the data using the leave-one-out strategy. Signature verification is a two class (genuine or fake) problem. Since the identity of the signature is already known, the nearest neighbour matching is only applied to the set of genuine and forged examples of the subject's signature. Our previous results using the linearity measure defined in [36] achieved 93.1% accuracy, which is now improved. Computing linearity of the $2D$ signatures using $\mathcal{L}(\mathcal{C})$ produces 97.2% accuracy. Note that applying dynamic time warping on pairs of $\mathcal{L}(\mathcal{C})$ linearity plots resulted in 96.0% accuracy, showing the ineffectiveness of warping in this context. For comparison, linearity was replaced by straightness, giving 96.9% accuracy, showing that $\mathcal{L}(\mathcal{C})$ provides a small improvement.

Fifth experiment ($3D$): Signature verification – improved accuracy. A further increase in accuracy in the signature verification task is obtained by assuming that the data samples along each signature were captured uniformly over time, and augmenting the $2D$ coordinates with time as the third dimension. That is, the data (x_t, y_t) is treated as $(x_t, y_t, \alpha t)$, where α is a scaling factor, and the $3D$ version of $\mathcal{L}(\mathcal{C})$ is applied. Two $3D$ signature examples are displayed in figure 16. The non-uniformity in the third dimension
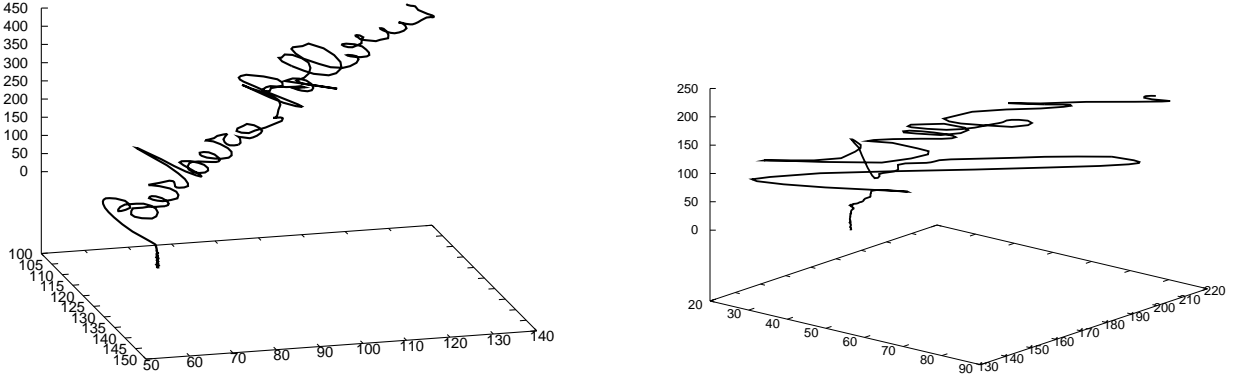
Figure 16: $3D$ versions of the leftmost signatures in figure 14.

can be most easily seen in the jump at the beginning of each signature.

In this experiment we use linearity plots assigned to $3D$ signatures. Figure 17 demonstrates the linearity plots for the signatures shown in figure 14. The plots in the first (second respectively) column contain the three genuine signatures from the upper (lower respectively) row in figure 14. The linearity plots in the third and fourth columns contain the forged versions. In general they display uniformity within each individual/writer, although the greater variability in the signatures in the second row of figure 14 is reflected in the corresponding (i.e. 2nd and 4th) linearity plots. Note that the inclusion of temporal information has increased the consistency of the second genuine set of signatures (compare the 2nd plot in figure 15 versus the 2nd plot in figure 17).

17

Figure 17: Examples of linearity plots for genuine signatures (leftmost two columns) and forged signatures (rightmost two columns). Linearity plots are provided for $3D$ versions of signatures, as displayed in figure 16.
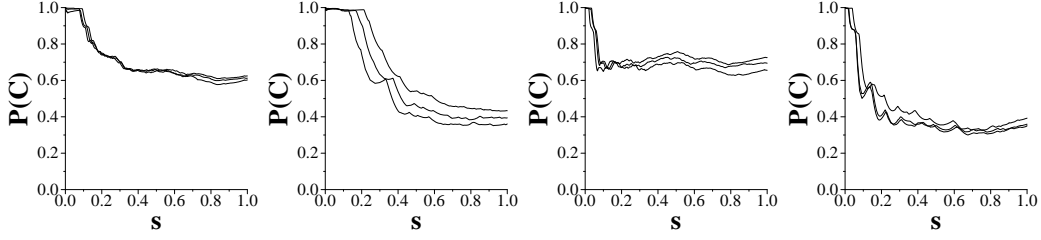
As in experiment 4, signature verification is carried out using nearest neighbour matching of each signature to the set of genuine and forged examples of that subjects signature. This time the linearity plots are computed from the $3D$ version of the signature data. The accuracy of 97.2% obtained by computing linearity of the $2D$ signatures using $\mathcal{L}(\mathcal{C})$ is marginally improved. With $\alpha = 0.2$ the signature verification accuracy becomes 97.8%, which is close to the accuracy of around 99% achieved by Munich and Perona's system that was specifically designed for signature analysis.

Sixth experiment ($3D$): Classifying 3D brain tracts. Four sets of brain fibre tracts, obtained by tractography from diffusion tensor imaging (DTI) scans of four subjects, are analysed. Each scan consists of bundles of 3D curves (between 1282 and 2683 tracts per subject), which were semi-automatically labelled into eight categories: left cingulum, right cingulum, corpus callosum, corticospinal, left fornix, right fornix, uncinate fasciculus, ushape (tracts connecting the cerebellar peduncles through the pons – these do not correspond to a standard anatomic structure, but are reproducible); see figure 18. 3D line moments were computed for each tract as a basic feature. Since subjects' heads are in a standard position when scanned, moment invariants were not necessary, and the ten raw moments up to second order were used. Classification was performed using an SVM [8] with a Radial Basis Function (RBF) kernel, and leave-one-out testing. Using just the moment features, the classification rate was 85.34%, which improved to 89.24% when the SVM used both the moments and linearity. In comparison, using moments and straightness instead of $\mathcal{L}(\mathcal{C})$ only produced a classification rate of 86.33%. Since the linearity and straightness measures provide somewhat different information they can be combined into the feature vector along with the moments. This produced a small improvement, achieving a classification rate of 91.27.

Seventh experiment (2D): The performance assessment in the presence of noise.
In this experiment we assess the performance of the new linearity measure in the presence of noise. The problems of sensitivity (some people would prefer to say "non-robustness" instead of "sensitivity") of the curve based methods in image processing and computer vision tasks are well recognized. The performance of curve based methods, depending on the noise level, can be strongly affected. On the other hand, the area based methods (in which all shape points, both boundary and interior ones, are involved in the computation)
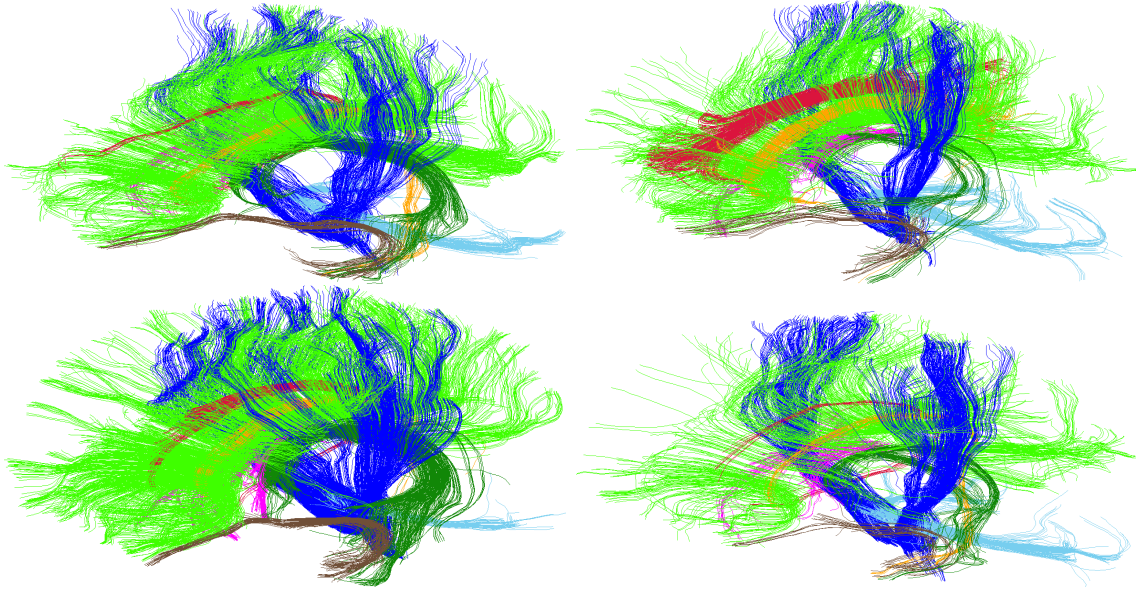
Figure 18: 3D tracts for four subjects with ground truth colour coding.

are more resistant to noise, or in general, small boundary deformations (like protrusions and intrusions). Of course, there are applications where preference can be given to either of these methods. For example, when working with low quality data, the preference would be given to the robust methods (i.e. area based ones). On the other hand, when working on high precision tasks the sensitivity property is preferred. For an analysis of the behaviour of the new measure in the presence of noise, we will use the same data set as used in the First Experiment, captured by Alimoğlu and Alpaydin [2] (consisting of 10978 handwritten digits (0 - 9)).

We start with a small sample set, displayed in Figure 19. Three digits are distorted by adding increasing amounts of normally distributed noise to each coordinate.

As the curves become more sinuous their linearity values decrease as expected, and do so in a stable manner. It can be seen that the addition of noise to the digits "1" and "4" has a similar effect on the straightness index. The digit "0" measured by the straightness index has shown the highest resistance to the presence of noise, which is actually as expected. In the ideal situation the digit "0" is represented by a closed curve, whose straightness index is equal to 0 and should not be changed after noise is added. In the presented situation, the digit "0" appears as a curve whose end points almost coincide, implying a very low (close to 0) value, which does not change much in the presence of noise.

The results of further analysis are demonstrated in figure 20 which shows test set classification accuracy when noise has been added to both the training and test data. We note that accuracy is not unduly affected by the addition of even substantial levels of noise. Both linearity and straightness provide similar levels of accuracy, and the combination of the two measures produces a substantial increase in classification accuracy. An overall higher classification accuracy by the straightness index can be explained by the fact that the straightness measure classifies "0" and "8" with a better accuracy, because both digits "0" and "8" (in a
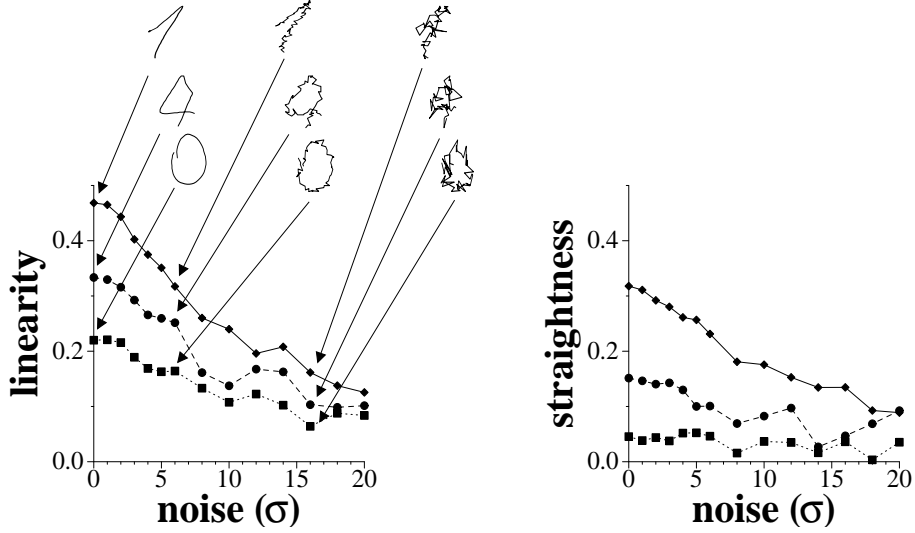
19

Figure 19: Effect of increasing amounts of noise on the measured linearity (on the left) and straightness values (on the right) for three digits: 0, 1, and 4.

perfect situation) are presented by closed curves and their straightness index is 0 – i.e., very close to zero if the selected data set is used. Since both will get a straightness value close to zero then the classification rate for these two digits will approach 50%, which is higher than the classification rate obtained for the other digits.[4]

It is very important to notice that, especially for relatively small noise levels, the combination of the two measures produces a substantial increase in classification accuracy. This shows that these two measures are compatible, and fairly independent. In simple words, the message from this experiment is: *Both linearity and straightness index are needed. The use of one does not preclude the use of the other.*

Table 2 shows the confusion matrix for the classification labels for the original (noise

---

[4]The straightness measure gives 54% and 45% classification rates for the digits "8" and "0" respectively, if no noise added. In a presence of noise, for $\sigma = 10$, these classification rates are 53% and 56%.
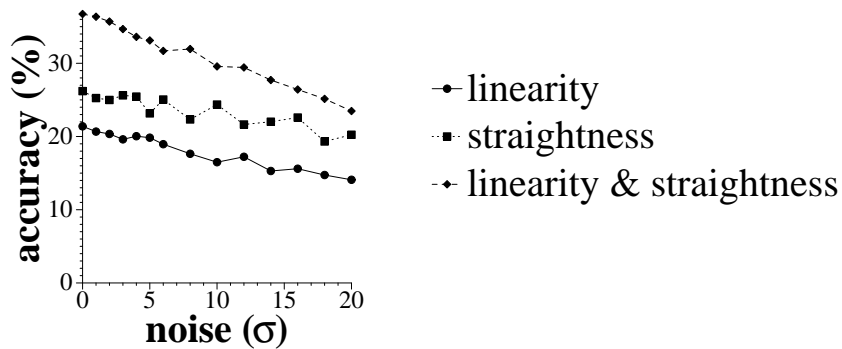

Figure 20: Effect of increasing amounts of noise on the accuracy of classifying 3493 test digits.

20

		Assigned Classes										total
		0	1	2	3	4	5	6	7	8	9	
True Classes	0	*32*	6	8	2	2	3	5	1	28	13	100
	1	10	*24*	9	10	6	12	7	6	8	9	100
	2	9	11	*12*	11	7	9	13	4	7	17	100
	3	1	11	11	*16*	12	15	14	7	1	13	100
	4	1	10	4	10	*19*	13	9	28	0	5	100
	5	2	14	10	14	12	*17*	11	13	1	6	100
	6	7	10	14	12	8	9	*15*	4	7	15	100
	7	3	7	5	7	23	7	4	*36*	1	6	100
	8	29	4	10	1	3	3	10	0	*28*	13	100
	9	12	8	16	11	6	7	15	4	7	*15*	100
	total	106	99	94	98	94	103	102	88	110	105	

Table 2: Confusion matrix for classification of test digits by the proposed linearity measure. Values have been scaled so that row values before rounding) sum to 100. Note that columns totals are also computed from the original data before rounding.

free) test data.[5] As expected, there is substantial confusion between certain classes (e.g. "0" and "8"; "2", "6" and "9"; "4" and "7"). When noise ($\sigma = 4$) is added to the data then, as expected, there is further confusion between additional classes, see the confusion matrix in table 3. Of course, as figure 21 demonstrates, the further added noise ($\sigma = 10$) has made many instances from different classes look similar to each other.

		Assigned Classes										total
		0	1	2	3	4	5	6	7	8	9	
True Classes	0	*26*	10	10	4	2	4	9	1	23	11	100
	1	11	*11*	10	8	13	11	10	13	7	6	100
	2	10	9	*12*	11	10	10	12	6	6	15	100
	3	5	13	16	*12*	10	15	10	9	4	7	100
	4	3	11	8	15	*13*	16	8	21	1	4	100
	5	5	15	10	12	15	*10*	7	13	4	10	100
	6	13	11	13	10	8	11	*14*	5	6	10	100
	7	5	11	3	9	19	13	7	*25*	2	5	100
	8	23	8	11	4	5	3	7	1	*24*	13	100
	9	15	8	13	6	5	11	12	3	10	*18*	100
	total	115	107	106	89	100	102	96	98	87	99	

Table 3: Confusion matrix for classification of test digits with added noise ($\sigma = 4$) by the proposed linearity measure. Values have been scaled so that row values (*before* rounding) sum to 100. Note that columns totals are also computed from the original data before rounding.

---

[5]The row and columns totals were computed from the original data which has subsequently been rounded for presentation, which explains the apparent small discrepancies in the totals.
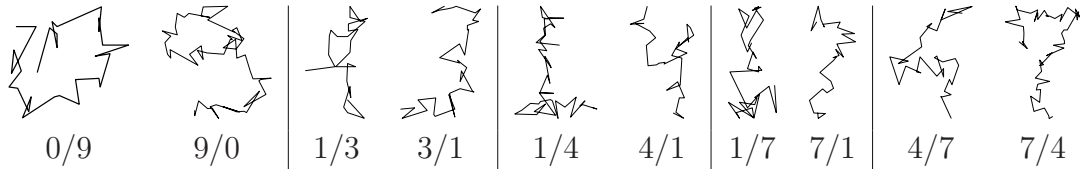
| 0/9 | 9/0 | 1/3 | 3/1 | 1/4 | 4/1 | 1/7 | 7/1 | 4/7 | 7/4 |

Figure 21: Misclassified test digits with added noise $\sigma = 10$ (the true class/assigned class is shown underneath).

Eighth experiment (2D): Combination of open curve and area based features.

The final experiments demonstrates that standard area based descriptors can be combined with our shape measure applied applied to open curves. We use the data set consisting of 808 *diatoms* from the ADIAC project, which have been manually labelled into 38 classes. Previously we have classified this data using several convexity measures both alone and in combination with the following set of descriptors [35]: circularity, ellipticity, rectangularity, triangularity [25] aspect ratio, compactness, convexity, eccentricity, the first four rotation, translation, and scale moment invariants, four rotation, translation, and scale moment invariants [28], the first three affine moment invariants [11]. For each diatom we have both the contour of its outer boundary and also the diatom's ornamentation, which consists of zero or more (mainly open) curve sections in the interior, see figure 22 for examples. We have rerun the classification task from [35], but in the current experiment, in addition to the convexity measures, the new linearity descriptor is applied individually to a diatom's interior curves, and for each diatom the weighted[6] mean and standard deviation of these linearity values is used as descriptors.[7] The remaining shape descriptors, which are a mixture of area and boundary based, are applied to the outer boundaries. Classification is performed using the nearest neighbour classifier with Mahalanobis distances.

As table 4 shows, the combination of linearity information from the open curves with the various area based and boundary based descriptors computed from the shape's boundary provides a consistent improvement in classification accuracy.[8]

6   Conclusion

This paper has described a new shape descriptor $\mathcal{L}(\mathcal{C})$ for computing the linearity of open curve segments in $2D$ and $3D$. Through the paper we have assumed that all curves have unit length and we then define the linearity measure as the sum of distances of the curve end points to the curve centroid. Of course, the assumption about the unit length of the curves considered is not a restriction in terms of applications in image processing and computer

---

[6]The interior curve's perimeter are used as the weighting term when calculating mean and standard deviation of linearity.

[7]For diatoms with no interior curves the mean and standard deviation linearity values are set to zero (there was a single such diatom in the set of 808).

[8]The classification results using convexity alone differ from the results reported in [35] since a different classifier is used in this paper which has improved performance.
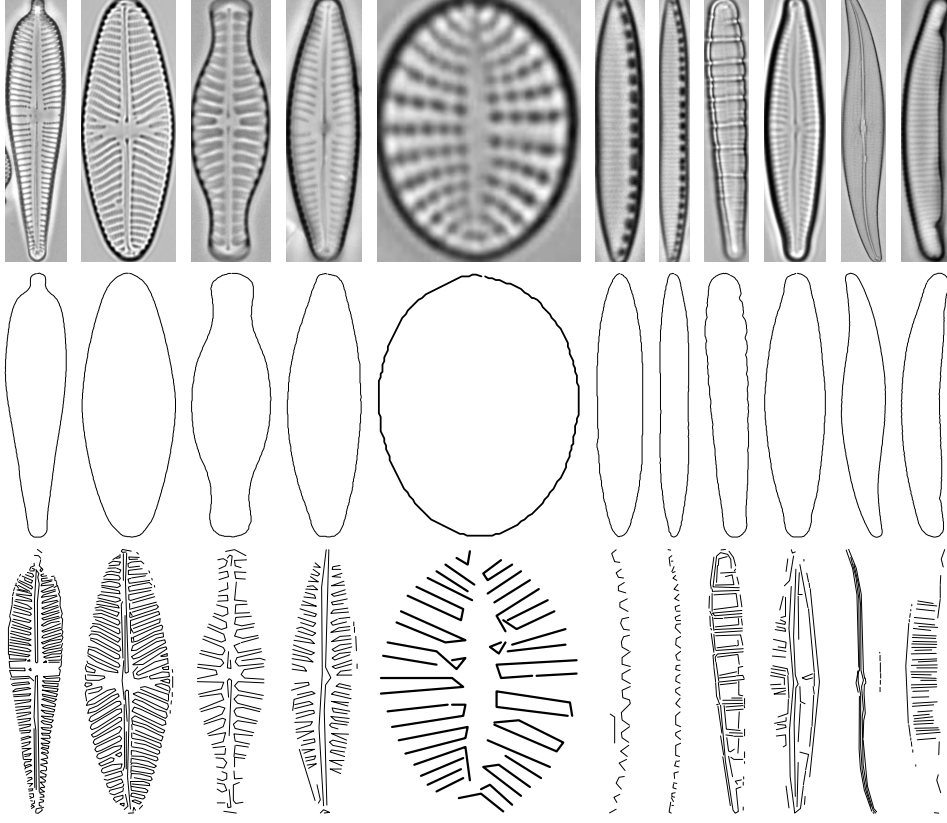
Figure 22: Diatoms ranked in increasing mean linearity of their internal contours. The top shows the original images, the middle row shows each diatom's external contour, and the bottom row shows the internal contours.

	$\mathcal{C}_2(S)$	$\mathcal{C}_3(S)$	$\mathcal{C}_{ZR}(S)$
convexity	16.83	11.26	16.83
convexity plus interior linearity	37.25	32.30	39.98
convexity and other features	87.75	86.88	87.75
convexity plus interior linearity and other features	88.99	90.47	88.24

Table 4: Classification accuracies for 808 diatoms using convexity plus additional shape features descriptors. The following convexity measures were used: $\mathcal{C}_2(S) = \frac{\text{area}(S)}{\text{area(convex hull}(S))}$, $\mathcal{C}_3(S) = \frac{\text{area(perimeter}(S))}{\text{perimeter}(S)}$, $\mathcal{C}_{ZR}(S)$ [35].

vision tasks. Indeed, if it is preferred to avoid such an assumption, then the new linearity measure $\mathcal{L}(\mathcal{C})$ can be computed as the ratio

$$\frac{\textit{Sum of distances of the curve end points to the curve centroid}}{\textit{Curve length}}$$

23

which is obviously an invariant with respect to the scaling transformations.

The new linearity measure is both very simple to implement and efficient to compute. It satisfies the basic requirements for a linearity measure:

- $\mathcal{L}(\mathcal{C})$ is in the interval $(0, 1]$;

- $\mathcal{L}(\mathcal{C})$ equals 1 only for straight line segments;

- $\mathcal{L}(\mathcal{C})$ is invariant with respect to translation, rotation and scaling transformation on a curve considered.

In addition, the new measure is theoretically well founded. All statements are accompanied with rigorous proofs. Supported by this, the behaviour of the new measure is well understood and predictable to some extent. This is an advantage since it enables a priori judgment regarding the measure's suitability for particular applications.

Experiments show the effectiveness of the new measure on several tasks. Some synthetic experiments are provided in order to illustrate that the new measure behaves in accordance with human perception (second experiment). Additional experiments are provided to illustrate the usefulness of the new measure in some application tasks. In the case of the signature verification, a high accuracy of 97.2% was achieved if the signatures are treated as $2D$ curves/objects. A further improvement of 97.8% was obtained when the signatures were treated as $3D$ objects (third coordinate/dimension is time-related and is derived based on an assumption that the signatures considered were captured uniformly over time). Taking into account that the new linearity measure was derived as a general classification/recognition tool such an achieved accuracy of 97.8% can be considered to be very high, even though it is slightly lower than the accuracy of around 99% obtained by a specially tailored system [20] for such signature analysis task.

Acknowledgement

References

[1] D.M. Acketa and J. Žunić. On the number of linear partitions of the (m, n)-grid. *Inf. Process. Lett.*, 38(3):163–168, 1991.

[2] F. Alimoğlu and E. Alpaydin. Combining multiple representations for pen-based handwritten digit recognition. *ELEKTRIK: Turkish Journal of Electrical Engineering and Computer Sciences*, 9(1):1–12, 2001.

[3] Marconi Barbosa, Riccardo Natoli, Kriztina Valter, Jan Provis, and Ted Maddess. Integral-geometry characterization of photobiomodulation effects on retinal vessel morphology. *Biomedical Optics Express*, 5(7):2317–2332, 2014.

24

[4] C. Beisbart, M. Barbosa, H. Wagner, and L. da F. Costa. Extended morphometric analysis of neuronal cells with Minkowsky valuations. *The European Physical Journal B*, 52(4):531–546, 2006.

[5] S. Benhamou. How to reliably estimate the tortuosity of an animal's path: straightness, sinuosity, or fractal dimension? *Journal of Theoretical Biology*, 229(2):209–220, 2004.

[6] E.T. Bowman, K. Soga, and T. Drummond. Particle shape characterisation using Fourier descriptor analysis. *Geotechnique*, 51(6):545–554, 2001.

[7] J. Canny. A computational approach to edge detection. *IEEE Trans. on Patt. Anal. and Mach. Intell.*, 8(6):679–698, 1986.

[8] Chih-Chung Chang and Chih-Jen Lin. LIBSVM: A library for support vector machines. *ACM Transactions on Intelligent Systems and Technology*, 2(3):27:1–27:27, 2011.

[9] C. Direkoglu and M.S. Nixon. Shape classification via image-based multiscale description. *Pattern Recognition*, 44(9):2134–2146, 2011.

[10] A. El-ghazal, O. Basir, and S. Belkasim. Farthest point distance: A new shape signature for Fourier descriptors. *Signal Processing: Image Communication*, 24(7):572–586, 2009.

[11] J. Flusser and T. Suk. Pattern recognition by affine moment invariants. *Pattern Recognition*, 26:167–174, 1993.

[12] T. Gautama, D.P. Mandić, and M.M. Van Hull. A novel method for determining the nature of time series. *IEEE Transactions on Biomedical Engineering*, 51(5):728–736, 2004.

[13] T. Gautama, D.P. Mandić, and M.M. Van Hulle. Signal nonlinearity in fMRI: A comparison between BOLD and MION. *IEEE Transactions on Medical Images*, 22(5):636–644, 2003.

[14] M. Hu. Visual pattern recognition by moment invariants. *IRE Trans. Inf. Theory*, 8(2):179–187, 1962.

[15] A.R. Imre. Fractal dimension of time-indexed paths. *Applied Mathematics and Computation*, 207(1):221–229, 2009.

[16] S. Manay, D. Cremers, B.-W. Hong, A. Yezzi, and S. Soatto. Integral invariants for shape matching. *IEEE Trans. on Patt. Anal. and Mach. Intell.*, 28(10):1602–1618, 2006.

[17] R. Melter, I. Stojmenović, and J. Žunić. A new characterization of digital lines by least square fits. *Pattern Recognition Letters*, 14(2):83–88, 1993.

[18] K. Michielsen and H. De Raedt. Integral-geometry morphological image analysis. *Physics Reports*, 347(6):461–538, 2001.

25

[19] W. Mio, A. Srivastava, and S.H. Joshi. On shape of plane elastic curves. *Int. Journal of Computer Vision*, 73(3):307–324, 2007.

[20] M.E. Munich and P. Perona. Visual identification by signature tracking. *IEEE Trans. on Patt. Anal. and Mach. Intell.*, 25(2):200–217, 2003.

[21] F. Pan and M. Keane. A new set of moment invariants for handwritten numeral recognition. In *Int. Conf. Image Processing*, pages 154–158, 1994.

[22] P. Pérez, M. Gangnet, and A. Blake. Poisson image editing. *ACM Trans. Graph.*, 22(3):313–318, 2003.

[23] E. Rahtu, M. Salo, and J. Heikkilä. A new convexity measure based on a probabilistic interpretation of images. *IEEE Trans. on Patt. Anal. and Mach. Intell.*, 28(9):1501–1512, 2006.

[24] P.L. Rosin. Edges: saliency measures and automatic thresholding. *Machine Vision and Applications*, 9(4):139–159, 1997.

[25] P.L. Rosin. Measuring shape: Ellipticity, rectangularity, and triangularity. *Machine Vision and Applications*, 14:172–184, 2003.

[26] C. Di Ruberto and A. Dempster. Circularity measures based on mathematical morphology. *Electronics Letters*, 36(20):1691–1693, 2000.

[27] H. Schweitzer and J. Straach. Utilizing moment invariants and Gröbner bases to reason about shapes. *Computational Intelligence*, 14(4):461–474, 1998.

[28] M. Sonka, V. Hlavac, and R. Boyle. *Image Processing, Analysis, and Machine Vision*. PWS, 1998.

[29] M. Stojmenović, A. Nayak, and J. Žunić. Measuring linearity of planar point sets. *Pattern Recognition*, 41(8):2503–2511, 2008.

[30] M. Stojmenović and J. Žunić. Measuring elongation from shape boundary. *Journal Mathematical Imaging and Vision*, 30(1):73–85, 2008.

[31] F. Valentine. *Convex Sets*. McGraw-Hill, New York, 1964.

[32] J. Žunić and C. Martinez-Ortiz. Linearity measure for curve segments. *Applied Mathematics and Computation*, 215(8):3098–3105, 2009.

[33] J. Žunić, J. Pantović, and P.L. Rosin. Measuring linearity of curves. In *Int. Conf. Pattern Recognition Applications and Methods - ICPRAM*, pages 388–395, 2013.

[34] J. Žunić and P.L. Rosin. Rectilinearity measurements for polygons. *IEEE Trans. on Patt. Anal. and Mach. Intell.*, 25(9):1193–3200, 2003.

[35] J. Žunić and P.L. Rosin. A new convexity measurement for polygons. *IEEE Trans. on Patt. Anal. and Mach. Intell.*, 26(7):923–934, 2004.

[36] J. Žunić and P.L. Rosin. Measuring linearity of open planar curve segments. *Image and Vision Computing*, 29(12):873–879, 2011.

[37] D. Zhang and G. Lu. Study and evaluation of different Fourier methods for image retrieval. *Image and Vision Computing*, 23(1):3349, 2005.